# Photoconductivity of Porphyrin Nanochannels Composed of Diprotonated Porphyrin Dications with Saddle Distortion and Electron Donors

Tatsuaki Nakanishi,[†] Takahiko Kojima,*[,†] Kei Ohkubo,[†] Taku Hasobe,[‡] Ken-ichi Nakayama,[†,§] and Shunichi Fukuzumi*[,†]

*Department of Material and Life Science, Graduate School of Engineering, Osaka University and SORST (JST), Suita, Osaka 565-0871, Japan, and School of Materials Science, Japan Advanced Institute of Science and Technology (JAIST) and PRESTO, JST, Nomi, Ishikawa 923-1292, Japan*

*Received September 12, 2008. Revised Manuscript Received October 24, 2008*

Supramolecular architecture named as porphyrin nanochannels (PNCs), including tetrathiafulvalene (TTF) and *p*-aminophenol as electron-donating guests in the inner space, was prepared with the hydrochloride salt of dodecaphenylporphyrin ($[H_4DPP]Cl_2$) by self-assembly based on intermolecular $\pi-\pi$ interactions. The crystal structure of the TTF-included PNC (PNC−TTF) was determined by X-ray crystallography. Intermolecular $\pi-\pi$ interaction was recognized among peripheral phenyl groups of the porphyrin, mainly in the direction of the crystallographic *c* axis to form a column structure. Photoinduced electron transfer from the guest molecules to $[H_4DPP]Cl_2$ occurred to give the electron-transfer state involving cation radicals of the guest molecules and one-electron reduced $[H_4DPP]Cl_2$, $\{[H_4DPP^{+\bullet}]Cl_2\}^-$, via the photoexcited singlet state of $[H_4DPP]Cl_2$ in PNC. The reactions were examined by solid-state femtosecond laser flash photolysis and ESR measurements to determine the rate constants of electron transfer and electronic structures of the cation radicals included in the cavity, respectively. A single crystal ($0.87 \times 0.23 \times 0.10$ mm$^3$) of PNC−TTF exhibited photoconductivity upon photoirradiation at 633 nm with a He−Ne laser (5 mW), and the photocurrent was 0.7 nA at electrical field strength of $3.5 \times 10^4$ V cm$^{-1}$. The photocurrent showed direction dependence toward the crystallographic *c* axis. This indicates that the intermolecular $\pi-\pi$ interaction is the main conduction pathway. Various PNC supramolecules including TTF and other electron-donating guest molecules were also employed to construct photoelectrochemical cells with use of $SnO_2$ transparent electrodes. Short-circuit photocurrent measurements were made on the cells with the OTE/$SnO_2$/PNC−guest photoanodes, and they exhibited clear photoresponse upon photoirradiation. The photocurrents increase with increasing the rate constants of the photoinduced electron transfer from the guest molecules to $[H_4DPP]Cl_2$, exhibiting saturation behavior. The performance of the cell with the OTE/$SnO_2$/PNC−TTF electrode exhibited the maximum IPCE (incident photon-to-current efficiency) value of 10.1% at 460 nm, which corresponded to the absorption maximum of the Soret band of $[H_4DPP]Cl_2$ on the electrode.

## Introduction

After the finding of organic conductors composed of tetrathiafulvalene (TTF; officially 2,2′-bis(1,3-dithiolylidene)) as an electron donor and tetracyanoquinodimethane (TCNQ) as an electron acceptor,[1,2] many kinds of crystalline materials with donor−acceptor conglomerates have been developed to improve conductivity in relation with characteristics of individual molecules and crystal engineering, which control the bulk molecular arrangements in the solid state.[3,4] On the other hand, organic semiconductors have also been developed to serve as an important subgroup toward construction of molecular devices involving organic field electric transistors.[5] Organic molecular semiconductors showing photoconductivity have been recognized as important components to develop well-organized photofunctional materials in nanometer scale, having been long-term objectives in the broad range of science.[6] In the solid state structures of organic conductors and semiconductors, weak noncovalent interactions including $\pi-\pi$ interactions play indispensable roles in terms of molecular ordering and construction of conduction pathways.[3b,7]

* Correspding authors: kojima@chem.eng.osaka-u.ac.jp (T.K.) and fukuzumi@chem.eng.osaka-u.ac.jp (S.F.).
[†] Osaka University and SORST (JST).
[‡] JAIST and PRESTO, JST.
[§] Present address: Department of Applied Chemistry, Graduate School of Science and Engineering, Yamagata University, Yonezawa, Yamagata 992-8510, Japan.

(1) Ferraris, J.; Cowan, D. O.; Walarka, V., Jr.; Peristein, J. H. *J. Am. Chem. Soc.* **1973**, *95*, 948.
(2) Coleman, L. B.; Cohen, M. J.; Sandman, D. J.; Yamagishi, F. G.; Garito, A. F.; Heeger, A. J. *Solid State Commun.* **1973**, *12*, 1125.
(3) (a) Bendikov, M.; Wudl, F. *Chem. Rev.* **2004**, *104*, 4891. (b) Segra, J. L.; Martín, N. *Angew. Chem., Int. Ed.* **2001**, *40*, 1372.
(4) Fraxedas, J. *Molecular Organic Materials*; Cambridge University Press: Cambridge, UK, 2006; Chapter 1.
(5) (a) Mas-Torrent, M.; Durkut, M.; Hadley, P.; Ribas, X.; Rovira, C. *J. Am. Chem. Soc.* **2004**, *126*, 984. (b) Mas-Torrent, M.; Hadley, P.; Bromley, S. T.; Ribas, X.; Tarres, J.; Mas, M.; Molins, E.; Veciana, J.; Rovira, C. *J. Am. Chem. Soc.* **2004**, *126*, 8546. (c) Sunder, V. C.; Zaumseil, J.; Podzorov, V.; Menard, E.; Willett, R. L.; Someya, T.; Gershenson, M. L.; Rogers, J. A. *Science* **2004**, *303*, 1644. (d) Tang, Q.; Li, H.; Liu, Y.; Hu, W. *J. Am. Chem. Soc.* **2006**, *128*, 14634. (e) Yamao, T.; Miki, T.; Akagami, H.; Nishimoto, Y.; Ota, S.; Hotta, S. *Chem. Mater.* **2007**, *19*, 3748. (f) Ashizawa, M.; Yamada, K.; Fukaya, A.; Kato, R.; Hara, K.; Takeya, J. *Chem. Mater.* **2008**, *20*, 4883.

10.1021/cm802460t CCC: $40.75 
Published on Web 11/20/2008

Porphyrins have been known to achieve self-assembly to form well-organized supramolecular structures by virtue of noncovalent interactions, mainly intermolecular $\pi-\pi$ interactions.[8] Porphyrins have been utilized as versatile photoresponsive building blocks of supramolecular assemblies via noncovalent interactions for photochemical energy conversion, for example, as mimics of the photosynthetic reaction center in photosystems.[9−12] Porphyrin assemblies have also gathered much attention as artificial photofunctional materials on the basis of intermolecular photoinduced electron transfer, and porphyrin nanostructures have been reported to exhibit photoconductivity in the solid state.[13−16] The photoconductivity in the porphyrin supramolecular architecture has been utilized to develop photovoltaic devices such as dye-sensitized solar cells.[17,18] In those photofunctional devices and materials, porphyrins and metalloporphyrin complexes usually act as electron donors.

Saddle distortion of porphyrin rings induced by intramolecular steric hindrance among peripheral substituents causes out-of-plane lone pairs of pyrroles to facilitate their protonation.[19] The protonation of porphyrins gives rise to the steric and electrostatic repulsion among the pyrrole N−H protons to enhance and fix the saddle distorted structure of porphyrin core, concomitant with hydrogen bond formation with counteranions.[20,21] The protonation of the pyrrole nitrogens in a porphyrin also results in large anodic shift of the reduction potential of the porphyrin ring.[22] This positive potential shift makes it possible for the protonated porphyrins to act as electron acceptors in photoinduced electron transfer. On the basis of this electron-accepting character of the protonated porphyrin, we reported on photoinduced electron transfer from electron-donating molecules such as hydroquinone derivatives to hydrochloride salt of saddle-distorted dodecaphenylporphyrin ($[H_4DPP]Cl_2$) which forms a porphyrin nanochannel (PNC) in the crystal phase to include electron-donating guest molecules in the inner cavity.[22,23] Thus, the PNC supramolecular assemblies are regarded as donor−acceptor organic materials.

In this article, we would like to report on the formation of PNC including stronger electron-donating guest molecules than hydroquinone derivatives such as TTF and *p*-aminophenol (*p*-AP), their enhanced photoconductivity in the crystal, and photovoltaic activity in the photoelectrochemical cells.

## Experimental Section

**Materials.** Chemicals were purchased from commercial sources and used without further purification, unless otherwise noted. Chloroform ($CHCl_3$) and acetonitrile ($CH_3CN$) used as solvents were distilled over $CaH_2$ before use. Toluene was distilled over sodium-benzophenone ketyl and used for synthesis of $H_2DPP$. Hydrochloride salt of $H_2DPP$ ($[H_4DPP]Cl_2$) was synthesized followed by literature procedures.[22] *p*-Aminophenol was sublimated before use.

**Preparation of Porphyrin Nanochannels.** A single crystal of PNC including tetrathiafulvalene (PNC−TTF) was obtained by recrystallization of $[H_4DPP]Cl_2$ (0.022 g, 0.017 mmol) and TTF (0.020 g, 0.098 mmol) from $CHCl_3/CH_3CN$ (= 1:1 v/v) solution under vapor diffusion of $CH_3CN$. Yield: 0.018 g, 71%. Anal. Calcd for $C_{95}H_{66}N_4Cl_2S_2 \cdot 2H_2O \cdot 2CH_3CN$: C, 78.40; H, 5.05; N, 5.54. Found: C, 78.31; H, 4.94; N, 5.79. $^1$H NMR ($CDCl_3$, $\delta$): 7.96 (d, 8H; *meso*-phenyl, *o-H*), 7.10 (t, 12H; *meso*-phenyl, *m-*, *p-H*), 6.68 (m, 40H; $\beta$-phenyl, *H*), 6.31 (d, 2H; $CH_2$ (TTF)), 2.31 (s, 4H; pyrrole-N*H*), 1.99 (s, 6H; $CH_3CN$), 1.51 (s, 4H, $H_2O$).

Single crystals of PNC containing *p*-aminophenol (*p*-AP) were obtained by the same method described above with use of

(6) (a) Vincent, V. M.; Wright, J. D. *J. Chem. Soc., Faraday Trans. 1* **1974**, *70*, 58. (b) Tamamura, T.; Yasuba, H.; Okamoto, K.; Imai, T.; Kusabayashi, S.; Mikawa, H. *Bull. Chem. Soc. Jpn.* **1974**, *47*, 448. (c) Silinsh, E. A.; Inokuchi, H. *Chem. Phys.* **1991**, *149*, 373. (d) Adam, D.; Schuhmacher, P.; Simmerer, J.; Häussling, L.; Siemensmeyer, K.; Etzbach, K. H.; Ringsdorf, H.; Haarer, D. *Nature* **1994**, *371*, 141.
(7) (a) Torrance, J. B. *Acc. Chem. Res.* **1979**, *12*, 79. (b) Inabe, T.; Tajima, H. *Chem. Rev.* **2004**, *104*, 5503.
(8) Hunter, C. A.; Sanders, J. K. M. *J. Am. Chem. Soc.* **1990**, *112*, 5525.
(9) For photosystems: (a) Ferreira, K. N.; Iverson, T. M.; Maghlaoui, K.; Barber, J.; Iwata, S. *Science* **2004**, *303*, 1831. (b) Jordan, P.; Fromme, P.; Witt, H. T.; Klukas, O.; Saenger, W.; Krau$\beta$, N. *Nature* **2001**, *411*, 909. (c) Barber, J. *Inorg. Chem.* **2008**, *47*, 1700.
(10) (a) Steinberg-Yfrach, G.; Liddell, P. A.; Hung, S.-C.; Moore, A. L.; Gust, D.; Moore, T. A. *Nature* **1997**, *385*, 239. (b) Gust, D.; Moore, T. A. In *The Porphyrin Handbook*; Kadish, K. M., Smith, K. M., Guilard, R., Eds.; Academic Press: New York, 2000; pp 153−190.
(11) (a) D'Souza, F.; Ito, O. *Coord. Chem. Rev.* **2005**, *249*, 1410. (b) D'Souza, F.; Chitta, R.; Gadde, S.; Zandler, M. E.; McCarty, A. L.; Sandanayaka, A. S. D.; Araki, Y.; Ito, O. *Chem.-Eur. J.* **2005**, *11*, 4416. (c) Choi, M.-S.; Aida, T.; Luo, H.; Araki, Y.; Ito, O. *Angew. Chem., Int. Ed.* **2003**, *42*, 4060.
(12) (a) Imahori, H.; Guldi, D. M.; Tamaki, K.; Yoshida, Y.; Luo, C.; Sakata, Y.; Fukuzumi, S. *J. Am. Chem. Soc.* **2001**, *123*, 6617. (b) Guldi, D. M.; Imahori, H.; Tamaki, K.; Kashiwagi, Y.; Yamada, H.; Sakata, Y.; Fukuzumi, S. *J. Phys. Chem. A* **2004**, *108*, 541. (c) Fukuzumi, S. *Bull. Chem. Soc. Jpn.* **2006**, *79*, 177.
(13) Schwab, A. D.; Smith, D. E.; Bond-Watts, B.; Johnston, D. E.; Hone, J.; Johnson, A. T.; de Paula, J. C.; Smith, W. F. *Nano Lett.* **2004**, *4*, 1261.
(14) Schouten, P. G.; Warman, J. W.; de Haas, M. P.; Fox, M. A.; Pan, H.-L. *Nature* **1991**, *353*, 736.
(15) (a) Liu, C.-Y.; Bard, A. J. *Nature* **2002**, *418*, 162. (b) Liu, C.-y.; Pan, H.-L.; Fox, M. A.; Bard, A. J. *Science* **1993**, *261*, 897. (c) Liu, C.-y.; Pan, H.-L.; Fox, M. A.; Bard, A. J. *Chem. Mater.* **1997**, *9*, 1422. (d) Fox, M. A.; Pan, H.-L.; Jones, W. E., Jr.; Melamed, D. *J. Phys. Chem.* **1995**, *99*, 11523. (e) Liu, C.-y.; Tang, H.; Bard, A. J. *J. Phys. Chem.* **1996**, *100*, 3587.
(16) (a) Wang, Q.; Wang, L.; Yu, J.; Yu, L. *Adv. Mater.* **2000**, *12*, 974. (b) Shimizu, Y.; Higashiyama, T.; Fuchita, T. *Thin Solid Films* **1998**, *331*, 279. (c) Araki, K.; Angnes, L.; Toma, H. E. *Adv. Mater.* **1995**, *7*, 554.
(17) (a) Hasobe, T.; Imahori, H.; Kamat, P. V.; Ahn, T. K.; Kim, S. K.; Kim, D.; Fujimoto, A.; Hirakawa, T.; Fukuzumi, S. *J. Am. Chem. Soc.* **2005**, *127*, 1216. (b) Hasobe, T.; Sandanayaka, A. S. D.; Wada, T.; Araki, Y. *Chem. Commun.* **2008**, 3372. (c) Hasobe, T.; Saito, K.; Kamat, P. V.; Troiani, V.; Qiu, H.; Solladie, N.; Kim, K. S.; Park, J. K.; Kim, D.; D'Souza, F.; Fukuzumi, S. *J. Mater. Chem* **2007**, *17*, 4160. (d) Hasobe, T.; Kamat, P. V.; Absalom, M. A.; Kashiwagi, Y.; Sly, J.; Crossley, M. J.; Hosomizu, K.; Imahori, H.; Fukuzumi, S. *J. Phys. Chem. B* **2004**, *108*, 12865. (e) Hasobe, T.; Imahori, H.; Yamada, H.; Sato, T.; Ohkubo, K.; Fukuzumi, S. *Nano Lett.* **2003**, *3*, 409. (f) Hasobe, T.; Kashiwagi, Y.; Absalom, M. A.; Sly, J.; Hosomizu, K.; Crossley, M. J.; Imahori, H.; Kamat, P. V.; Fukuzumi, S. *Adv. Mater.* **2004**, *16*, 975.
(18) (a) Cho, Y.-J.; Ahn, T. K.; Song, H.; Kim, K. S.; Lee, C. Y.; Seo, W. S.; Lee, K.; Kim, S. K.; Kim, D.; Park, J. T. *J. Am. Chem. Soc.* **2005**, *127*, 2380. (b) Liu, C.-y.; Bard, A. J. *J. Am. Chem. Soc.* **1998**, *120*, 5575.
(19) (a) Senge, M. O. *Chem. Commun.* **2006**, 243. (b) Nurco, D. J.; Medforth, C. J.; Forsyth, T. P.; Olmstead, M. M.; Smith, K. M. *J. Am. Chem. Soc.* **1996**, *118*, 10918. (c) Medforth, C. J.; Senge, M. O.; Smith, K. M.; Sparks, L. D.; Shelnutt, J. A. *J. Am. Chem. Soc.* **1992**, *114*, 9859.
(20) Stone, A.; Fleischer, E. B. *J. Am. Chem. Soc.* **1968**, *90*, 2735.
(21) Kojima, T.; Honda, T.; Ohkubo, K.; Shiro, M.; Kusukawa, T.; Fukuda, T.; Kobayashi, N.; Fukuzumi, S. *Angew. Chem., Int. Ed.* **2008**, *47*, 6712.
(22) (a) Kojima, T.; Nakanishi, T.; Harada, R.; Ohkubo, K.; Yamauchi, S.; Fukuzumi, S. *Chem.-Eur. J.* **2007**, *13*, 8714. (b) Harada, R.; Kojima, T. *Chem. Commun.* **2005**, 716. (c) Kojima, T.; Nakanishi, T.; Honda, T.; Fukuzumi, S. *J. Porphyrins Phthalocyanines*, in press, 2009.
(23) Fukuzumi, S.; Kojima, T. *J. Mater. Chem.* **2008**, *18*, 1427.

**Table 1. X-ray Crystallographic Data for PNC−TTF**

| | |
|---|---|
| compound | PNC−TTF |
| formula | $C_{99}H_{72}Cl_2N_6S_2O_2$ |
| fw | 1512.72 |
| crystal system | monoclinic |
| space group | *C*2/*c* (No. 15) |
| *T*, K | 123 |
| *a*, Å | 17.411(1) |
| *b*, Å | 25.125(2) |
| *c*, Å | 19.436(2) |
| *β*, deg | 108.493(4) |
| *V*, Å$^3$ | 8063(1) |
| *Z* | 4 |
| no. of reflections measured | 17481 |
| no. of observations | 5807 |
| no. of parameters refined | 502 |
| $R1^a$ | 0.0904 ($I > 2\sigma(I)$), 0.1525 (all data) |
| $Rw^{b,c}$ | 0.2218 (all data) |
| GOF | 1.290 |

$^a$ $R1 = \sum||F_o| - |F_c||/\sum|F_o|$. $^b$ $Rw = [\sum(w(F_o^2 - F_c^2)^2)/\sum w(F_o^2)^2]^{1/2}$. $^c$ $w = 1/[\sigma^2(F_o^2) + (0.0500P)^2 + 30.0000P$, where $P = (\max(F_o^2, 0) + 2F_c^2)/3$.

$[H_4DPP]Cl_2$ (0.021 g, 0.016 mmol) and *p*-AP (0.022 g, 0.20 mmol) in place of TTF. Yield: 0.020 g, 80%. Anal. Calcd for $C_{98}H_{71}N_5O \cdot 2CH_3CN \cdot 0.5CHCl_3$: C, 79.56; H, 5.05; N, 6.34. Found: C, 79.73; H, 5.05; N, 6.44. $^1$H NMR ($CDCl_3$, $\delta$): 7.96 (d, 8H; *meso*-phenyl, *o-H*), 7.10 (t, 12H; *meso*-phenyl, *m-*, *p-H*), 6.68, 6.55 (m, 44H; *β*-phenyl, *H* and phenyl *H* (*p*-AP)), 2.25 (s, 4H; pyrrole-N*H*), 2.00 (s, 6H; $CH_3CN$).

A single crystal of guest-free PNC (PNC−water) was obtained by recrystallization of $[H_4DPP]Cl_2$ as described previously.[22a]

**X-ray Crystallographic Measurements for PNC−TTF.** A single crystal of PNC−TTF was mounted on a glass capillary with silicon grease. All measurements were performed on a Rigaku Mercury CCD area detector at −150 °C with graphite-monochromated Mo Kα radiation ($\lambda = 0.71070$ Å) up to $2\theta_{max} = 54.7°$. The structure was solved by direct methods and expanded using Fourier techniques. All non-hydrogen atoms were refined anisotropically, except for TTF and a cluster composed of four molecules of $H_2O$ having 0.5 population, respectively. Refinement was carried out with full-matrix least-squares on *F* with scattering factors[24] and including anomalous dispersion effects.[25] All calculation were performed using the Crystal Structure crystallographic software package[26] and structure refinements were made by using SHELX-97.[27] Crystallographic data are summarized in Table 1.

**Physical Measurements.** X-band ESR spectra were recorded on a JEOL JES-ME-LX spectrometer at room temperature with photoirradiation by a USHIO USH1005D high-pressure mercury arc lamp (1000 W) equipped with a water filter to avoid infrared irradiation and a glass cutoff filter ($\lambda > 340$ nm). Single crystals were used as the sample of PNC−TTF and PNC−(*p*-AP). ESR sample tubes (4.5 mm) charged with the samples were degassed and sealed under Ar. ESR measurements were performed under nonsaturating microwave power conditions. The amplitude of modulation was chosen to optimize the resolution and the signal-to-noise (*S*/*N*) ratio of the observed spectra. Simulations of ESR signals were made by using a WinSIM program[28] to determine the hyperfine coupling constants and maximum slope linewidths.

NMR spectra were recorded on a JEOL A-300 spectrometer, and chemical shifts were determined relative to the residual solvent peaks. The fluorescence spectra of single crystals of PNC−TTF and PNC−water were measured by using absolute PL quantum yield measurement system (Hamamatsu photonics Co., Ltd., C9920-02) by excitation at 500 nm.

Femtosecond transient absorption spectroscopy experiments in potassium bromide (KBr) pellets were conducted using an ultrafast source: Integra-C (Quantronix Corp.), an optical parametric amplifier, TOPAS (Light Conversion Ltd.), and a commercially available optical detection system, Helios, provided by Ultrafast Systems LLC. The source for the pump and probe pulses were derived from the fundamental output of Integra-C (780 nm, 2 mJ/pulse and fwhm = 130 fs) at a repetition rate of 1 kHz. A total of 75% of the

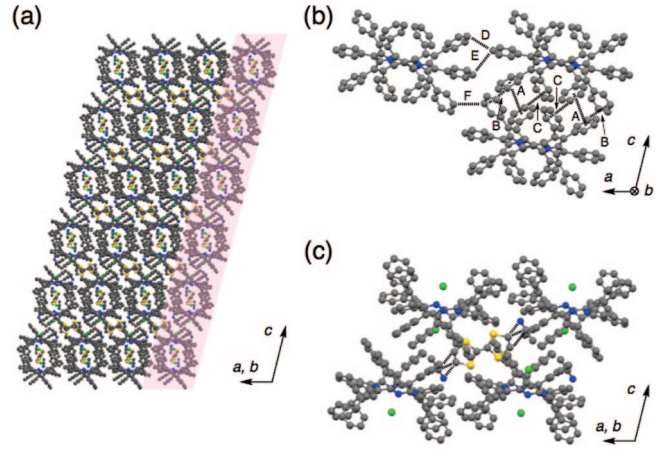


**Figure 1.** Crystal structure of PNC−TTF (carbon: gray, nitrogen: blue, sulfur: yellow, chlorine: light green): (a) crystal packing with column structure indicated by pink shade; (b) intermolecular $\pi-\pi$ interactions in the crystal indicated by dotted lines. Interatomic distances: A, 3.39, 3.48, 3.50, 3.53, 3.54, 3.60 Å; B, 3.69 Å; C, 3.66 Å; D, 3.63 Å; E, 3.53 Å; F, 3.58 Å; (c) intermolecular $\pi-\pi$ interaction between TTF and $CH_3CN$ indicated by dotted lines. Interatomic distances: 3.49, 3.51, 3.66 Å.

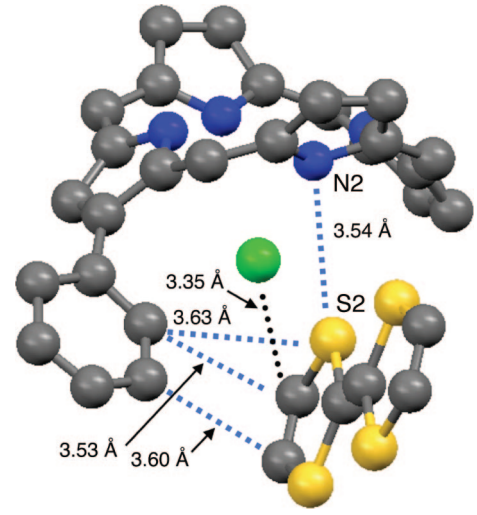


**Figure 2.** Intermolecular interactions between the saddle-distorted $H_4DPPCl_2$ and TTF in the PNC−TTF. Peripheral phenyl groups except an interacting *β*-phenyl group are omitted for clarity. Arrow (black) represents hydrogen bonding and dashed lines (gray) represent $\pi-\pi$ interactions.

(24) Creagh, D. C.; McAuley, W. J. In *International Tables for Crystallography*; Wilson, A. J. C., Ed.; Kluwer Academic Pulishers: Boston, 1992; vol. *C*, Table 4.2.6.8, pp 219−222.
(25) Ibers, J. A.; Hamilton, W. C. *Acta Crystallogr.* **1964**, *17*, 781.
(26) *Crystal Structure 3.8.2*, Crystal Structure Analysis Package; Rigaku and Rigaku/MSC: The Woodlands, TX, 2000−2008.
(27) Sheldrick, G. M. *SIR 97 and SHELX 97, Programs for Crystal Structure Refinement*; University of Göttingen: Göttingen, Germany, 1997.
(28) The WinSIM program is developed at the NIEHS by Duling (URL: http://www.niehs.nih.gov/research/resources/software/tools/index.cfm): Duling, D. R. *J. Magn. Res. Ser. B* **1994**, *104*, 105.

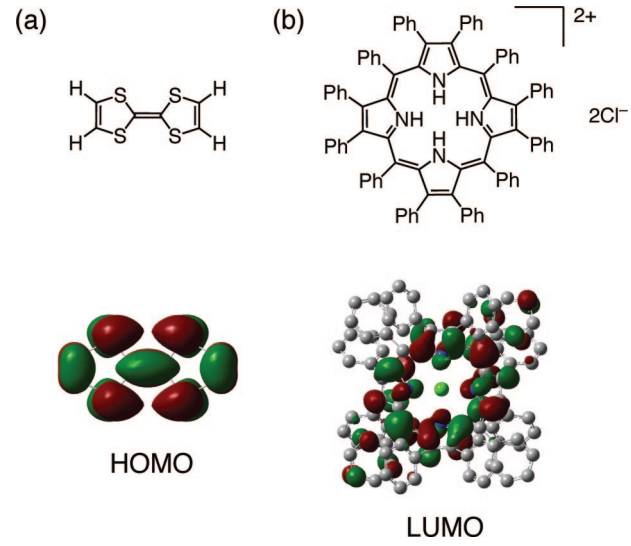


**Figure 3.** Schematic descriptions of (a) TTF and (b) $[H_4DPP]Cl_2$ together with their HOMO (B3LYP/6−31G(d) level) and LUMO orbitals (B3LYP/6-31G level), respectively.

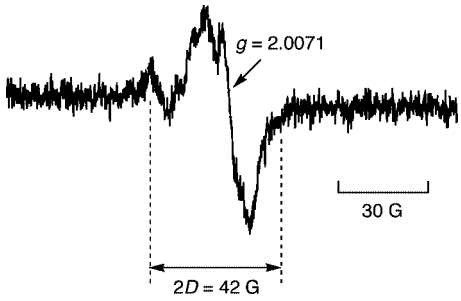


**Figure 4.** ESR spectrum observed upon photoirradiation ($\lambda$ > 340 nm) of crystals of PNC−TTF at 25 °C.

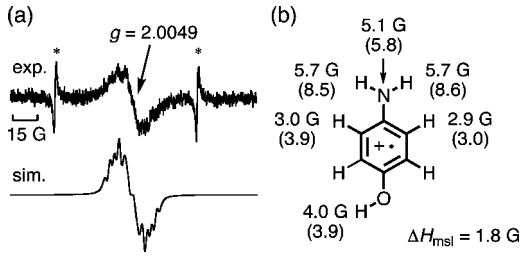


**Figure 5.** (a) ESR spectrum of *p*-$AP^{+\bullet}$ formed in PNC−(*p*-AP) upon photoirradiation ($\lambda$ > 340 nm) and its computer simulation. Asterisks denote $Mn^{2+}$ marker; (b) hyperfine coupling constants and the maximum slope of line width ($\Delta H_{msl}$) used for the simulation and calculated hyperfine coupling constants obtained by DFT calculations in parentheses.

fundamental output of the laser was introduced into TOPAS which has optical frequency mixers resulting in tunable range from 285 to 1660 nm, while the rest of the output was used for white light generation. Prior to generating the probe continuum, a variable neutral density filter was inserted in the path to generate stable continuum, and then the laser pulse was fed to a delay line that provides an experimental time window of 3.2 ns with a maximum step resolution of 7 fs. In our experiments, a wavelength at 355 nm of TOPAS output, which is the fourth harmonic of signal or idler pulses, was chosen as the pump beam. As this TOPAS output consists of not only desirable wavelength but also unnecessary wavelengths, the latter was deviated using a wedge prism with wedge angle of 18°. The desirable beam was irradiated at the sample cell with a spot size of 1 mm diameter where it was merged with the white probe pulse in a close angle (<10°). The probe beam after passing through the 2 mm sample cell was focused on a fiber optic cable that was connected to a CCD spectrograph for recording the time-resolved spectra (410−800 nm). Typically, 2500 excitation pulses were averaged for 5 s to obtain the transient spectrum at a set delay time. Kinetic traces at appropriate wavelengths were assembled from the time-resolved spectral data. All measurements were performed using KBr pellets containing porphyrin nanochannel at 295 K.

**Photocurrent Measurements on a Single Crystal of PNC−TTF.** Photocurrent measurements for a single crystal (0.87 × 0.23 × 0.10 $mm^3$) of PNC−TTF were performed by the two-terminal method using gold paste (Tokuriki Chemical Research, SILBEST No. 8560) and gold wire (Tanaka Denshi Kogyo Co., Ltd., 50 $\mu$m $\phi$) with an electrometer (Keithley Instruments Inc., model 6517A) under photoirradiation by using He−Ne laser (633 nm, 5 mW) and from AM 1.5 conditions simulated solar light (Yamashita Denso Co., Ltd., YSS-50A).

**Preparation of PNC-Deposited Films.** Preparation of OTE coated with the nanostructured $SnO_2$ film is as follows. A dilute (∼5%) $SnO_2$ colloidal aqueous solution (Alpha Chemicals, particle size: ∼15 nm) was repeatedly sprayed onto the OTE electrode (FTO film from Ceramic Forum, Japan, sheet resistance: ∼8 Ω/square), followed by annealing at 673 K for ∼0.5 h. The OTE coated with the nanostructured $SnO_2$ film is referred to as OTE/$SnO_2$.[17] Porphyrin crystal-deposited films were simply prepared by drop-cast method. A 1 mL suspension of porphyrin crystal (1 mM) in diethyl ether was dropped onto substrates (OTE/$SnO_2$, surface area: 5 mm × 5 mm) and then dried in air.

**Measurements of Photocurrents in Photoelectrochemical Solar Cells.** Photoelectrochemical measurements were carried out in a standard two-compartment cell consisting of a working electrode and a Pt wire gauze counter electrode in the electrolyte. The electrolyte is 0.5 M LiI and 0.01 M $I_2$ in $CH_3CN$. KEITHLEY 2400 was used for recording photocurrent generation response and IPCE action spectra. A collimated light beam from a 300 W xenon lamp with an AM 1.5 filter was used for excitation of the porphyrin assembly film deposited on OTE/$SnO_2$. In the case of IPCE measurements, a monochromator (SM-25, Bunkoh-Keiki Co., Ltd) was introduced into the path of the excitation beam for the selected wavelength. The lamp intensity at each wavelength was determined by Si photodiode (Hamamatsu Photonics S1337-1010BQ) and corrected.

**Theoretical Calculations.** Density functional calculations[29] were performed with Gaussian03 (Revision C.02, Gaussian, Inc.).[30] DFT calculations on TTF and *p*-AP were performed on a 32-processor QuantumCube at B3LYP/6-31G(d) level of theory and DFT-calculations of crystal structure of $H_4DPPCl_2$ were performed on an 8-processor QuantumCube at B3LYP/6-31G level of theory. Graphical outputs of the computational results were generated with the Gauss View software program (ver. 3.09) developed by Semichem, Inc.[31]

## Results and Discussion

**Crystal Structure of PNC−TTF.** Crystallization of $[H_4DPP]Cl_2$ in the presence of 6 equiv of TTF from $CHCl_3$ with vapor diffusion of $CH_3CN$ afforded green single crystals of porphyrin nanochannel including TTF in the inner space

(29) (a) Becke, A. D. *J. Chem. Phys.* **1993**, *98*, 5648. (b) Lee, C.; Yang, W.; Parr, R. G. *Phys. Rev. B* **1988**, *37*, 785.
(30) Frisch, M. J.; et al. *Gaussian 03*, Revision C.02; Gaussian, Inc.: Wallingford, CT, 2004. The full list of authors is given in the Supporting Information.
(31) Dennington, R., II; Keith, T.; Millam, J.; Eppinnett, K.; Hovell. W. L.; Gilliland, R. Semichem, Inc.: Shawnee Mission, KS, 2003.

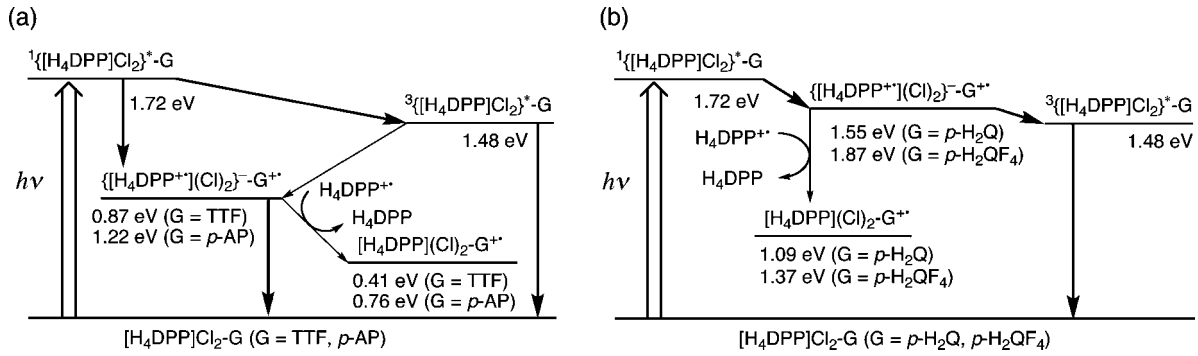


**Figure 6.** (a) Energy diagram of PNC−TTF and PNC−(*p*-AP); (b) energy diagram of PNC−(*p*-$H_2Q$) and PNC−(*p*-$H_2QF_4$).

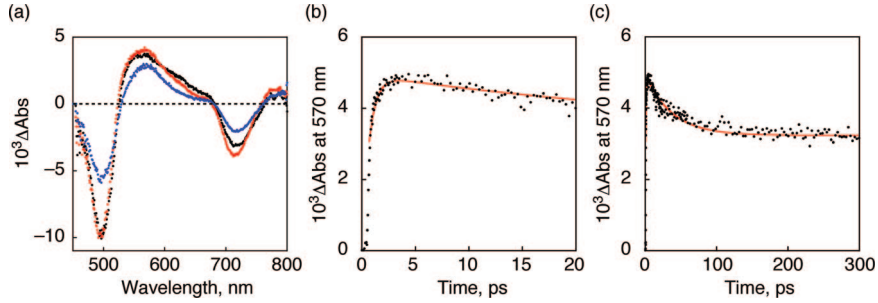


**Figure 7.** (a) Transient absorption spectra in fs-LFP for PNC−TTF in KBr pellet; at 1.5 ps (black line), at 20 ps (red line), and at 3000 ps (blue line) after photoexcitation at 355 nm. (b and c) Time profiles of the absorbance at 570 nm; (b) 0−20 ps and (c) 0−300 ps, respectively.

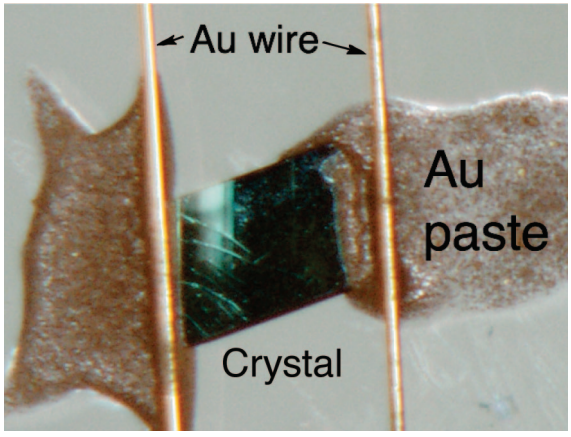


**Figure 8.** Sample manipulation for photoconductivity measurements of a single crystal of PNC−TTF.

of the channel structure. The crystal structure of the porphyrin nanochannel including TTF (PNC−TTF) is depicted in Figure 1. PNC−TTF exhibits a column structure along with the crystallographic *c* axis as indicated by colored shadow in Figure 1a by virtue of intermolecular $\pi-\pi$ interactions among peripheral phenyl groups. In the column, face-to-face $\pi-\pi$ interactions denoted as A and edge-to-face $\pi-\pi$ interactions denoted as B and C were found as *intracolumn* $\pi-\pi$ interaction. All these interactions are formed among phenyl groups attached at the $\beta$-positions of pyrroles of [$H_4$DPP]$Cl_2$. Parallel to the crystallographic *ab* plane, weaker intermolecular $\pi-\pi$ interactions denoted as D, E, and F were observed as *intercolumn* $\pi-\pi$ interaction. In addition, the TTF molecule also formed intermolecular $\pi-\pi$ interaction with $CH_3CN$ in the cavity as shown in Figure 1c.

The population of the TTF molecule included in the PNC was estimated to be 0.5, and the other half of the cavity was occupied by a cluster of four molecules of water forming hydrogen bonding network. Thus, the PNC−TTF consists of [$H_4$DPP]$Cl_2$, two molecules of $CH_3CN$, and a TTF molecule as formulated to be [$H_4$DPP]$Cl_2$·0.5TTF·2$H_2O$·2$CH_3CN$. The population of TTF relative to the $H_4DPP^{2+}$ ion was confirmed by $^1$H NMR spectroscopy which allowed us to determine 2:1 ratio of $H_4DPP^{2+}$/TTF by peak integration of a singlet due to the vinyl protons of TTF at 6.31 ppm and a doublet assigned to the *o*-protons of the *meso* phenyl groups of $H_4DPP^{2+}$ at 7.96 ppm. Further addition of TTF resulted in no change in the ratio of 2:1 for $H_4DPP^{2+}$:TTF. This is probably due to the larger molecular size of TTF compared to those of hydroquinone derivatives and *p*-AP.[22] Comparison of the cell parameters of the single crystals of PNC supramolecules including guest molecules revealed that the PNC−TTF exhibited the longest *b* among the crystallographically characterized PNCs: the *b* value for the PNC−TTF was 25.125(2) Å; however, those of others fell in the range of 24.4826(19)−24.7840(10) Å.[22] Since the PNC architecture can be formed regardless of the presence or absence of guest molecules which are appropriate in size to be included,[22] the PNC structure is assumed to be the thermodynamic minimum for the self-assembly of [$H_4$DPP]$Cl_2$. Thus, the larger TTF molecule compels steric enforcement to enlarge the inclusion site in the PNC structure to cause the structural strain. This structural bias may result in the half-occupancy of the TTF molecules in the guest inclusion site.

The driving force of the inclusion of TTF into PNC is $\pi-\pi$ interaction with $H_4DPP^{2+}$ as indicated by the interatomic distances between S2···N2 (3.539(4) Å) and that between TTF and one $\beta$-phenyl group (Figure 2). The $\pi-\pi$ interaction via the sulfur of TTF and the nitrogen of the

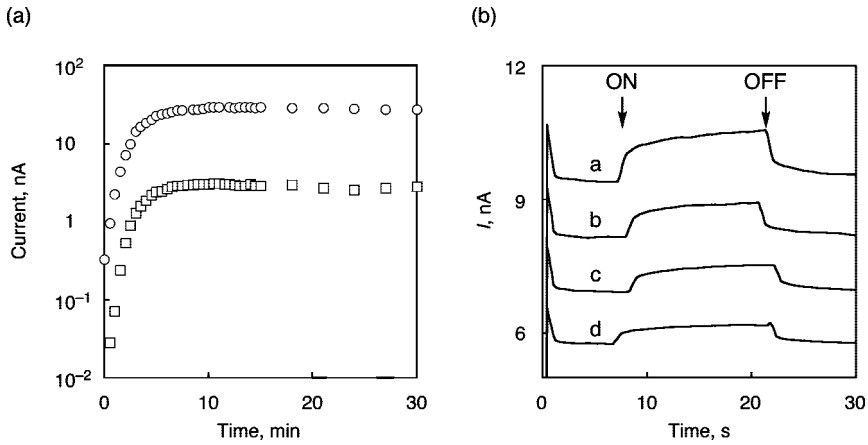


**Figure 9.** (a) Direction dependence of photocurrent under AM 1.5 illumination at room temperature: parallel to the crystallographic *c* axis (circle) and perpendicular to the *c* axis (square). (b) Photocurrent response for a single crystal of PNC−TTF upon photoexcitation at 633 nm by He−Ne laser (in the direction of the crystallographic *c* axis) under various electrical field strengths: a, $3.5 \times 10^4$ V cm$^{-1}$; b, $3.1 \times 10^4$ V cm$^{-1}$; c, $2.6 \times 10^4$ V cm$^{-1}$; d, $2.1 \times 10^4$ V cm$^{-1}$.

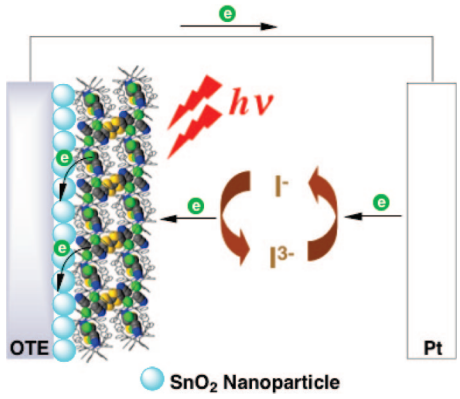


**Figure 10.** Schematic description of a photoelectrochemical cell using OTE/$SnO_2$/PNC−TTF anode.

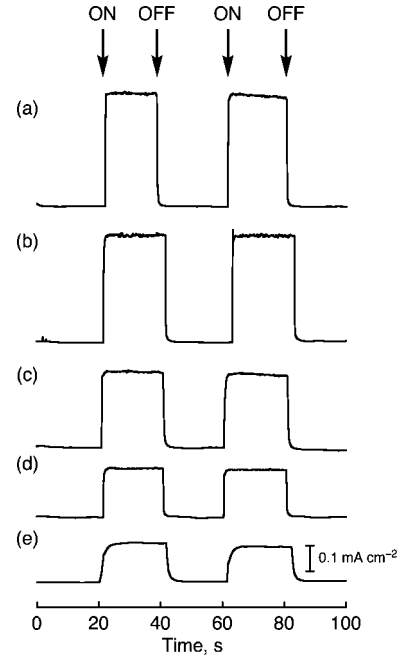


**Figure 11.** Photocurrent response of OTE/$SnO_2$/PNC electrodes observed for (a) PNC−TTF, (b) PNC−(*p*-AP), (c) PNC−(*p*-$H_2Q$), (d) PNC−(*p*-$H_2QF_4$), and (e) PNC−water under AM 1.5 illumination at room temperature (∼100 mW cm$^{-2}$).

pyrrole moiety in $[H_4DPP]Cl_2$ should be particularly important to perform efficient electron transfer from TTF to the singlet excited-state of $[H_4DPP]Cl_2$, $^1\{[H_4DPP]Cl_2\}$*, since the HOMO of TTF resides in the sulfur atoms dominantly and the LUMO of $[H_4DPP]Cl_2$ involves nitrogen 2p orbitals as shown in Figure 3 to give rise to HOMO−LUMO interaction.

**Photoinduced Electron Transfer in PNC−TTF.** The diffuse reflection spectrum of PNC−TTF exhibited the absorption maxima at 488 and 724 nm, which were the same as those observed for other PNC supramolecular assemblies including various guest molecules.[22a] Although the solid-state fluorescence spectrum ($\lambda_{ex} = 500$ nm) of PNC−water that contains only water molecules as guests in the channel showed the emission maximum at 870 nm ($\phi = 0.005$), no fluorescence was observed for the PNC−TTF in the solid state (see Figure S1 in Supporting Information). This result suggests that the singlet excited-state of $[H_4DPP]Cl_2$ moiety in the PNC−TTF is quenched by photoinduced electron transfer from TTF to $[H_4DPP]Cl_2$.

Upon photoirradiation ($\lambda > 340$ nm) of single crystals of PNC−TTF in an ESR cavity, we could observe an signal a $g = 2.0071$ as shown in Figure 4. This signal can be assigned to that of $TTF^{+\bullet}$ which is a one-electron oxidized species of TTF.[32] In addition, we could observe a signal due to a triplet biradinal, $(TTF^{+\bullet})_2$, for which the *D* value was determined to be 21 G. On the basis of this value, the distance between the two coupled $TTF^{+\bullet}$ radicals is estimated to be 11.0 Å, which is in good agreement with that found in the crystal structure (10.8 Å).[33] This result clearly indicates that photoinduced electron transfer occurs from the TTF molecules included to the $H_4DPP^{2+}$ moiety; however, the ESR signal due to the one-electron reduced species of $[H_4DPP]Cl_2$, $\{[H_4DPP^{+\bullet}]Cl_2\}^-$, was not detected due to electron hopping to undergo disproportionation as described previously.[22]

(32) (a) Wudl, F.; Smith, G. M.; Hufnagel, E. J. *J. Chem. Soc., Chem. Commun.* **1970**, 1453. (b) Matsubayashi, G.; Yokoyama, K.; Tanaka, T. *J. Chem. Soc., Dalton Trans.* **1988**, 253.

(33) The distance (*r*, Å) between the two radical center was estimated by the following equation: $r = [(2.78 \times 10^4)/D]^{1/3}$.

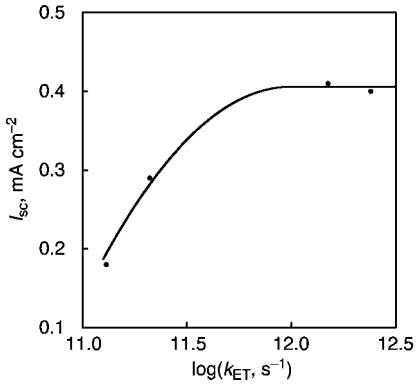


**Figure 12.** Plot of $I_{SC}$ relative to log($k_{ET}$) for PNC−guest.

In the case of PNC−(*p*-AP), we could observe an ESR signal assigned to *p*-AP$^{+\bullet}$ at $g = 2.0049$ as given in Figure 5a. The simulation of the spectrum on the basis of DFT calculations at the B3LYP/6-31G(d) level of theory allowed us to assign hyperfine coupling constants using the maximum slope linewidth ($\Delta H_{msl}$) of 1.8 G as shown in Figure 5b. This result also demonstrates the occurrence of photoinduced electron transfer from *p*-AP to [$H_4$DPP]$Cl_2$.

The energy of the singlet excited state of [$H_4$DPP]$Cl_2$ ($^1${[$H_4$DPP]$Cl_2$}*) has been determined to be 1.72 eV from the absorption and fluorescence maxima of PNC−water as mentioned above. The one-electron oxidation potential of TTF was determined by cyclic voltammetry measurements in dichloromethane ($CH_2Cl_2$, 0.1 M [(*n*-butyl)$_4$N]$PF_6$ as an electrolyte) at room temperature to be 0.41 V relative to SCE. Since the reduction potential has been reported to be −0.46 V (vs SCE),[22a] the driving force of the electron transfer from TTF to $^1${[$H_4$DPP]$Cl_2$}* is determined to be 0.87 eV. Similarly, we determined oxidation potentials of other guest molecules: 0.76 V for *p*-AP, 1.09 V for *p*-$H_2$Q, and 1.37 V for *p*-$H_2QF_4$. On the basis of these data, we determined the energy levels of the corresponding electron-transfer states of PNC−guests: 1.22 eV for PNC−*p*-AP, 1.55 eV for PNC−*p*-$H_2$Q, and 1.87 eV for PNC−*p*-$H_2QF_4$. An energy diagram of PNCs including guest molecules, for which the energy level of the electron-transfer state is lower than that of the triplet excited state of [$H_4$DPP]$Cl_2$ ($^3${[$H_4$DPP]$Cl_2$}*, is shown in Figure 6a, and that is also given in Figure 6b, for which the energy level of the electron-transfer state is higher than that of $^3${[$H_4$DPP]$Cl_2$}*. The energy of the electron-transfer state for PNC−(*p*-$H_2QF_4$) determined from the reduction potential of [$H_4$DPP]$Cl_2$ and the oxidation potential of *p*-$H_2QF_4$ in $CH_2Cl_2$ was higher than that of $^1${[$H_4$DPP]$Cl_2$}*; however, electron transfer took place. The actual oxidation potential of *p*-$H_2QF_4$ in PNC may be lower than that of *p*-$H_2QF_4$ in $CH_2Cl_2$ due to OH/$\pi$ interaction between hydroxyl group of *p*-$H_2QF_4$ and pyrrole ring of $H_4DPP^{2+}$.[22a]

Femtosecond laser flash photolysis (fs-LFP) was performed on the crystals of PNC−TTF in a KBr pellet at room temperature with photoexcitation at 355 nm, and transient absorption spectra are depicted in Figure 7a. At 1.5 ps after laser pulse, we could observe a transient absorption spectrum of $^1${[$H_4$DPP]$Cl_2$}* at 560 nm (black line in Figure 7a).[22a] The spectrum of the singlet excited-state changed to exhibit an absorption at 580 nm at 20 ps after laser illumination. We assigned the absorption at 580 nm to the one-electron oxidized species of TTF ($TTF^{+\bullet}$) on the basis of the reported spectrum of $TTF^{+\bullet}$.[34] The one-electron reduced species of [$H_4$DPP]$Cl_2$, {[$H_4DPP^{+\bullet}$]$Cl_2$}$^-$, has been reported to exhibit the absorption maximum at 530 nm. The rise of absorption at 530 nm was also observed; however, the bleaching of the Soret band suppressed the increase of the absorption. This observation indicates that electron transfer indeed occurs from TTF to $^1${[$H_4$DPP]$Cl_2$}* to produce an electron-transfer state involving $TTF^{+\bullet}$ and {[$H_4$DPP]$Cl_2$}$^-$ in the PNC−TTF supramolecular architecture.

In the transient absorption spectrum observed at 3000 ps after laser pulse, we could observe a transient absorption with the absorption maximum at 570 nm (the blue line in Figure 7a). The absorption maximum of $^3${[$H_4$DPP]$Cl_2$}* has been reported to be observed at 560 nm in benzonitrile.[22a] Since the ratio of $H_4DPP^{2+}$/TTF in PNC−TTF is 2:1, remaining $^1${[$H_4$DPP]$Cl_2$}* that does not react with TTF undergoes intersystem crossing to afford $^3${[$H_4$DPP]$Cl_2$}*. Thus, the spectrum observed for PNC−TTF as the blue line in Figure 7a can be ascribed to the long-lived $^3${[$H_4$DPP]$Cl_2$}*.

The change of transient absorption spectra of PNC−TTF was analyzed by using a double exponential function to determine the rates of the electron transfer reaction to generate the electron-transfer state and the sum of the rates of the intersystem crossing to give $^3${[$H_4$DPP]$Cl_2$}* and the back electron transfer to go back from electron-transfer state to the ground-state of $H_4DPP^{2+}$. The rise of absorbance at 570 nm was followed to determine the electron-transfer rate constant to be $1.5 \times 10^{12}$ s$^{-1}$ as shown in Figure 7b.

The electron-transfer state decayed with the rate constant of $2.7 \times 10^{10}$ s$^{-1}$ based on the analysis of the double exponential function as shown in Figure 7c. This decay of the electron-transfer state may involve both the back electron transfer and intersystem crossing processes.

We also conducted fs-LFP to determine the rate constants for PNC−(*p*-AP) in a KBr pellet (Figure S2, Supporting Information). The generation of the electron-transfer state involving *p*-AP$^{+\bullet}$ and {[$H_4DPP^{+\bullet}$]$Cl_2$}$^-$ was observed via the formation of $^1${[$H_4$DPP]$Cl_2$}* with the rate constant of $2.4 \times 10^{12}$ s$^{-1}$, which was larger than that observed for PNC−TTF, even though the driving force of the photoinduced electron transfer was smaller than that for PNC−TTF. This is probably due to intermolecular hydrogen bonding in the PNC, which makes the oxidation potential of *p*-AP lower than that of TTF.

**Photoconductivity in the Single Crystal of PNC−TTF.** Photocurrent measurements were made by a two-terminal method using gold paste and gold wire (50 $\mu$m $\phi$) as shown in Figure 8.

Photocurrent response under AM 1.5 illumination is demonstrated in Figure 9a. The photocurrent exhibited direction dependence in the single crystal. When the electric voltage was applied along with the crystallographic *c* axis,

(34) Torrance, J. B.; Scott, B. A.; Welber, B.; Kaufman, F. B.; Seiden, P. E. *Phys. Rev. B* **1979**, *19*, 730.

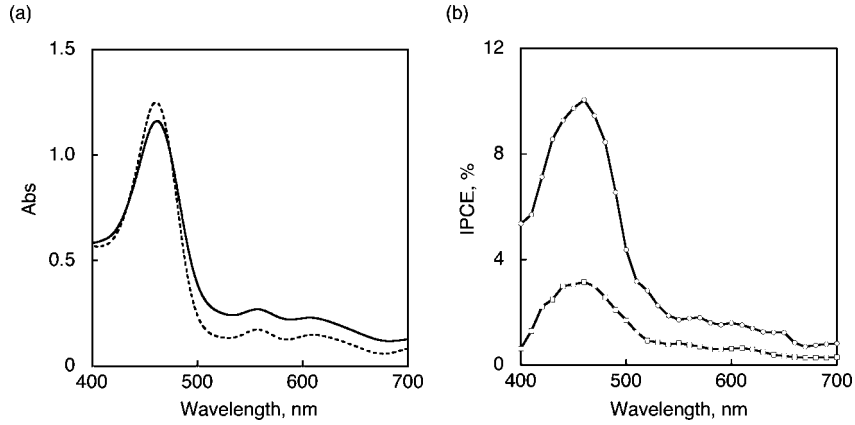


**Figure 13.** (a) Absorption spectra of OTE/$SnO_2$/PNC−TTF (solid line) and OTE/$SnO_2$/PNC−water (dotted line); (b) IPCE plots for OTE/$SnO_2$/PNC−TTF (circle) and OTE/$SnO_2$/PNC−water (square).

**Table 2. Short Circuit Photocurrent ($I_{SC}$) for PNC−Guests in Photoelectrochemical Cells**

| | PNC−TTF | PNC−(*p*-AP) | PNC−(*p*-$H_2$Q) | PNC−(*p*-$H_2QF_4$) | PNC−water |
|---|---|---|---|---|---|
| $I_{SC}$ (mA $cm^{-2}$) | 0.41 | 0.40 | 0.29 | 0.18 | 0.13 |
| $V_{OC}$ (mV) | 240 | 220 | 180 | 150 | 120 |
| $E_{ox}$ (V vs SCE) of electron donor[a] | 0.41 | 0.76 | 1.09[d] | 1.37[d] | (1.11)[e] |
| $-\Delta G_{ET}$[b] | 0.87 | 1.22 | 1.55[d] | 1.83[d] | (1.57)[f] |
| $k_{ET}$ ($s^{-1}$) | $1.5 \times 10^{12}$ | $2.4 \times 10^{12}$ | $2.1 \times 10^{11}$[d] | $1.3 \times 10^{11}$[d] | NA[g] |
| HOMO (eV)[c] | −4.57 | −4.99 | −5.41[d] | −6.19[d] | |

[a] Determined by CV for TTF and SHACV for others in $CH_2Cl_2$ (0.1 M $TBAPF_6$ as an electrolyte) at room temperature under Ar. [b] $-\Delta G_{ET} = -(E_{ox}(\text{guest}) - E_{red}([H_4DPP]Cl_2))$, where $E_{red}([H_4DPP]Cl_2) = -0.46$ (V vs SCE). [c] Calculated at the B3LYP/6-31G(d) level of theory. [d] Ref 22a. [e] The oxidation potential of $[H_4DPP]Cl_2$. [f] Determined relative to the oxidation potential of $[H_4DPP]Cl_2$. [g] Not available.

the photocurrent reached to 26 nA.[35] On the other hand, when the electric voltage was applied along the direction perpendicular to the crystallographic *c* axis, the maximum of photocurrent was 2.9 nA, which was only ca. 1/10 compared with that observed in the direction of the *c* axis.[35] As described in Figures 1 and 2, the intermolecular $\pi-\pi$ interaction among $H_4DPP^{2+}$ units was found mainly along with the crystallographic *c* axis for the $\beta$-phenyl groups. This result clearly indicates that the main conduction path is the *intracolumn* $\pi-\pi$ interactions among the $\beta$-phenyl groups. The *intercolumn* $\pi-\pi$ interaction among phenyl groups is, thus, suggested to exhibit partial contribution to the photoconduction in the PNC supramolecular assemblies.

We could observe photocurrent response upon turn-on and turn-off of photoirradiation with He−Ne laser (5 mW, 633 nm). The photocurrent in the direction of the crystallographic *c* axis increased in accordance with increase in the electrical field strength in the range of $2.1 \times 10^4$ to $3.5 \times 10^4$ V $cm^{-1}$ as shown in Figure 9b. At the field strength of $3.5 \times 10^4$ V $cm^{-1}$ (trace a in Figure 9b), we observed 0.7 nA of photocurrent as the maximum value. The photocurrent in the direction perpendicular to the crystallographic *c* axis was too small to be detected. This indicates that the photocurrent is not due to thermal hopping of electrons but the photoinduced hopping of electrons in principle.

**Photoelectrochemical Properties of OTE/$SnO_2$/PNC−Guests.** In order to evaluate the photoelectrochemical performance of the PNC supramolecules, we prepared various OTE/$SnO_2$/PNC electrodes as photoanodes in photoelectrochemical cells. The photoactive materials are PNC supramolecular assemblies including various guest molecules, such as TTF, *p*-AP, *p*-hydroquinone (*p*-$H_2$Q), and *p*-tetrafluorohydroquinone (*p*-$H_2QF_4$). We also employed PNC including $H_2O$ as the guest molecules (PNC−water) as a reference. Schematic description of the photoelectrochemical cell is shown in Figure 10.

We performed short circuit photocurrent ($I_{SC}$) and photovoltage response ($V_{OC}$) measurements on those OTE/$SnO_2$/PNC electrodes immersed into a $CH_3CN$ solution containing 0.5 M of LiI and 0.01 M of $I_2$ as electrolytes using a Pt gauze counter electrode.[17] The rate constants of electron transfer for the guest molecules are the most plausible parameters to evaluate the feasibility of oxidation of the guest molecules rather than their redox potentials in solution. The photocurrent response is prompt, steady, and reproducible during repeated on/off cycles of the visible light illumination as shown in Figure 11. A plot $I_{SC}$ vs $\log(k_{ET})$ ($k_{ET}$ stands for rate constant of electron transfer) is depicted in Figure 12. The $I_{SC}$ values exhibit saturation to reach the maximum of 0.41 mA $cm^{-2}$ observed for PNC−TTF.[36]

Finally, we examined the performance of the photoelectrochemical cell using the OTE/$SnO_2$/PNC−TTF anode as a solar cell. Absorption spectra of the OTE/$SnO_2$/PNC−TTF

(35) Gradual increase of the currents in the crystal indicates the partial contribution from thermal conduction to the photocurrent given in Figure 9a under AM 1.5 conditions.

(36) The $V_{oc}$ values are also shown in Table 2. With an increase in $k_{ET}$, the respective $V_{oc}$ values increase. This indicates that ultrafast formation of the charge-separated state contributes to the enhanced charge-injection into $SnO_2$ nanocrystallites. Therefore, the trend of $I_{sc}$ is largely dependent on $k_{ET}$ values. The photovoltage response of OTE/$SnO_2$/PNC−TTF electrode under AM 1.5 illumination is also shown in Figure S3, Supporting Information. See the following reference papers: (a) Subramanian, V.; Wolf, E. E.; Kamat, P. V. *J. Am. Chem. Soc.* **2004**, *126*, 4943. (b) Hasobe, T.; Murata, H.; Kamat, P. V. *J. Phys. Chem. C* **2007**, *111*, 16626.

and the OTE/$SnO_2$/PNC−water electrodes exhibited absorption maxima at 462, 557, and 607 nm for the former and 461, 557, and 610 nm for the latter as depicted in Figure 13a.[37] The incident photon-to-current efficiency (IPCE) values at various excitation wavelengths were determined from the following equation (eq 1),[38]

$$\text{IPCE}\ (\%) = (I_{SC}/I_{inc})(1240/\lambda) \times 100 \qquad (1)$$

where $I_{inc}$ is the incident light intensity (W $cm^{-2}$) and $\lambda$ is the excitation wavelength (nm). The action spectra of both the OTE/$SnO_2$/PNC−TTF and the OTE/$SnO_2$/PNC−water electrodes are shown in Figure 13b. The close match in the absorption and action spectra was observed to indicate that the singlet excited-state of $[H_4DPP]Cl_2$ is responsible for the photocurrent generation which should stem from the photoinduced electron transfer from the electron-donating guest molecules to $^1\{[H_4DPP]Cl_2\}^*$ followed by intermolecular electron hopping. The IPCE value for the OTE/$SnO_2$/PNC−TTF electrode exhibited the maximum value of 10.1% at 460 nm, which corresponded to the absorption maximum of the Soret band. The maximum IPCE value of the OTE/$SnO_2$/PNC−water anode was 3.1% at 460 nm. Thus, the maximum IPCE value for the OTE/$SnO_2$/PNC−TTF is more than three times higher than that of the OTE/$SnO_2$/PNC−water.

## Summary

We have demonstrated that porphyrin nanochannels including electron-donating guest molecules exhibit photoconductivity in the supramolecular assemblies. This functionality arises from the photoinduced electron transfer from the included guest molecules to the singlet excited-state of $[H_4DPP]Cl_2$ that acts as an electron acceptor. Solid-state fs-LFP and ESR spectroscopies clearly indicate the formation of the cation radical of the guest molecule as a one-electron oxidized species and $\{[H_4DPP^{+\bullet}]Cl_2\}^-$ as a one-electron reduced species. The latter undergoes disproportionation in the crystal via intermolecular electron-hopping, and this disproportionation gives rise to the photocurrent under certain electrical field strength and in the photoelectrochemical cells. The photocurrent exhibited clear direction-dependence in the single crystal; the 10-times larger photocurrent was observed toward the direction of the crystallographic *c* axis than that in the *ab* plane. Scrutiny into the crystal structures of PNC−guests revealed that the intermolecular $\pi-\pi$ interactions among the $\beta$-phenyl groups of $H_4DPP^{2+}$ are dominantly formed into the crystallographic *c* axis to form a column, which are connected with each other via intermolecular $\pi-\pi$ interactions. The direction dependence indicates that the electron conduction path of the photocurrent should be the $\pi-\pi$ interactions among phenyl groups to facilitate electron hopping. The cell using ITO/$SnO_2$/PNC−TTF exhibited the maximum IPCE value of 10.1% by photoirradiation at 460 nm. The finding described here will pave a way to construction of multicomponent photofunctional conglomerates based on self-assembled porphyrin nanoarchitectures.

**Acknowledgment.** This work was supported by a Grant via "Potentiality verification stage" program from Japan Science and Technology Agency, Grants-in-Aid (Nos. 18033033, 19205019, 19655045, and 19750034), and a Global COE program, "the Global Education and Research Center for Bio-Environmental Chemistry", from the Ministry of Education, Culture, Sports, Science and Technology, Japan. T.N. appreciates support from a JSPS predoctral fellowship (No. A208410). T.H. acknowledges special coordination funds for promoting science and technology from MEXT.

**Supporting Information Available:** Crystallorgaphic data for PNC−TTF (CIF format), solid-state fluorescence spectra of PNC−water and PNC−TTF, transient absorption spectra and time profile for PNC−(*p*-AP), and the full list of authors for ref 30 (PDF). This material is available free of charge via the Internet at http://pubs.acs.org.

CM802460T

(37) After the photocurrent measurements on the photoelectrochemical cells, the PNC samples supported on the electrodes were extracted with $CHCl_3$ to measure absorption spectra. The spectra were consistent with that of $[H_4DPP]Cl_2$ to confirm that no decomposition occurred during the measurements.

(38) Khazraji, A. C.; Hotchandani, S.; Das, S.; Kamat, P. V. *J. Phys. Chem. B* **1999**, *103*, 4693.